



**HAL**  
open science

## Rheological characterization of $\beta$ -lactoglobulin/lactoferrin complex coacervates

Rima Soussi Hachfi, Marie-Hélène Famelart, Florence Rousseau, Pascaline Hamon, Said Bouhallab

► **To cite this version:**

Rima Soussi Hachfi, Marie-Hélène Famelart, Florence Rousseau, Pascaline Hamon, Said Bouhallab. Rheological characterization of  $\beta$ -lactoglobulin/lactoferrin complex coacervates. *LWT - Food Science and Technology*, 2022, 163, pp.113577. 10.1016/j.lwt.2022.113577 . hal-03682487v1

**HAL Id: hal-03682487**

**<https://hal.inrae.fr/hal-03682487v1>**

Submitted on 31 May 2022 (v1), last revised 8 Jun 2022 (v2)

**HAL** is a multi-disciplinary open access archive for the deposit and dissemination of scientific research documents, whether they are published or not. The documents may come from teaching and research institutions in France or abroad, or from public or private research centers.

L'archive ouverte pluridisciplinaire **HAL**, est destinée au dépôt et à la diffusion de documents scientifiques de niveau recherche, publiés ou non, émanant des établissements d'enseignement et de recherche français ou étrangers, des laboratoires publics ou privés.



Distributed under a Creative Commons Attribution - NonCommercial - NoDerivatives 4.0 International License



## Rheological characterization of $\beta$ -lactoglobulin/lactoferrin complex coacervates

Rima Soussi Hachfi, Marie-Hélène Famelart, Florence Rousseau, Pascaline Hamon, Saïd Bouhallab\*

INRAE, Institut Agro, STLO, 65 Rue de Saint Briec, F-35042, Rennes, France

### ARTICLE INFO

#### Keywords:

Food heteroprotein  
Viscoelasticity  
Rheology  
Liquid-liquid phase separation

### ABSTRACT

Heteroprotein complex coacervation between lactoferrin (LF) and  $\beta$ -lactoglobulin ( $\beta$ -LG), two oppositely charged proteins from whey, occurred under specific conditions of pH, ionic strength and protein molar ratio. The present work aims at characterizing the rheological properties of the concentrated phase called coacervate obtained after phase separation. Unlike some polysaccharide/protein coacervates,  $\beta$ -LG/LF heteroprotein coacervates exhibit a liquid-like behavior; the loss modulus  $G''$  being 100 times higher than the storage modulus  $G'$  at low frequencies. This behavior was confirmed under creep-recovery tests. The heteroprotein coacervates exhibited a Newtonian viscous flow under low shear rate and a shear thinning behavior above  $10 \text{ s}^{-1}$ . The coacervates are exceptionally viscous, reaching a viscosity value of  $55 \pm 10 \text{ Pa}\cdot\text{s}$  which is  $\sim 2500$  times higher than that measured on individual protein solutions of equivalent total concentration. Also, a structural change occurred in the coacervates, probably due to the weaknesses of electrostatic interactions inside the protein network at high shear rates. The observed time-dependent structural rearrangement was proved to be reversible. These findings open new ways for the use of coacervates as texturizing agents in food matrices.

### 1. Introduction

Complex coacervation is an electrostatically and entropically-driven associative liquid-liquid phase separation (LLPS) process which most often takes place between two oppositely charged macromolecules (Kizilay, Kayitmazer, & Dubin, 2011). Since the pioneer research on complex coacervation of gelatine and gum Arabic by Bungenberg De Jong and Kruyt one century ago (Bungenberg De Jong & Kruyt, 1929), the biopolymer-based coacervates continue to be a fundamental research focus. Nowadays, the research programs on complex coacervation and more generally on LLPS are burgeoning not only in order to generate new materials and new applications for food or pharmaceutical industries but also to understand the intra-cellular biological assemblies and the origin of some neurodegenerative diseases (For more details, see reviews by Croguennec, Tavares, & Bouhallab, 2017; Yewdall, André, Lu, & Spruijt, 2021; Kapelner, Yeong, & Obermeyer, 2021). The main promising applications for food and pharmaceutical industries are macromolecular purification, encapsulation for protection and delivery of bioactives and nutrients and also elaboration of biomaterials with new textures and functionalities (Blocher & Perry, 2017; Croguennec

et al., 2017).

The generic process of complex coacervation leading to LLPS can be summarized into four main steps: initially, a spontaneous attractive interaction between macromolecules of opposite charges leads to formation of primary units whose stoichiometry is system dependent (Croguennec et al., 2017). Then, the formation of soluble complexes from these primary units (building blocks) according to a not completely elucidated mechanism. The third step is the growth step with the formation of micrometric droplets characteristic of complex coacervation (Wang, Zhang, & Tian, 2021) and finally, the coalescence of these droplets with gentle LLPS into a dense phase (coacervates) and dilute phase (Jho, Yoo, Lin, Han, & Hwang, 2017).

Various research works allowed progress in the understanding of the mechanisms of the complex coacervation. However, the vast majority are centred on proteins/polysaccharides, proteins/synthetic polyelectrolytes and polyelectrolytes/polyelectrolytes mixtures. Studies focusing on complex coacervation involving proteins of opposite charge, called heteroprotein complex coacervation (HPCC) are more recent and therefore less well documented (Croguennec et al., 2017; Zheng, Tang, & Sun, 2020).

\* Corresponding author.

E-mail address: [said.bouhallab@inrae.fr](mailto:said.bouhallab@inrae.fr) (S. Bouhallab).

<https://doi.org/10.1016/j.lwt.2022.113577>

Received 16 February 2022; Received in revised form 12 May 2022; Accepted 16 May 2022

Available online 19 May 2022

0023-6438/© 2022 The Authors. Published by Elsevier Ltd. This is an open access article under the CC BY-NC-ND license (<http://creativecommons.org/licenses/by-nc-nd/4.0/>).

As recently reviewed, HPCC constitutes a special case of LLPS because its process is highly sensitive to the ionic strength, occurs at narrow range of pH and follows the principle of charge and size compensation (Boire et al., 2018). Indeed, the formed dense phase is composed of at least two different proteins with opposite charges. During this last decade, several couples of oppositely charged proteins, from both animal and plant origins, were used to understand the main mechanism that drives HPCC (Croguennec et al., 2017). These different works have mainly focused on the optimal conditions for HPCC, the properties of primary units and the formed micrometric droplets, but little on the structural characterization of the final dense phase.

The HPCC based on two milk proteins, Lactoferrin (LF) and  $\beta$ -lactoglobulin ( $\beta$ LG), is the most studied system (Anema & de Kruijff, 2014; Chapeau et al., 2016; Kizilay et al., 2014; Tavares, Croguennec, Hamon, Carvalho, & Bouhallab, 2015). These studies provided several fundamental elements on i- the physico-chemical conditions for optimal complex coacervation including pH, ionic strength, stoichiometry and protein surface charge, ii- the molecular nature of the primary units; iii- the structure of formed  $\beta$ LG-LF droplets and their ability to encapsulate a bioactive molecule. Moreover, two studies have attempted to characterize the structure and properties of the final coacervates by combining SAXS and rheology (Kizilay et al., 2014) or Fluorescence recovery after photo-bleaching and solid state NMR (Peixoto et al., 2016). They concluded that the coacervate phase is a dynamic network with a complex molecular composition. The aim of the present work is to extend these studies by a combination of rheological methods for in-depth characterization of the coacervates formed between  $\beta$ LG and LF. Rheological analysis provides insight into the internal structure of biomaterials very useful for potential processing (Abraham, Sharika, Mishra, & Thomas, 2017).  $\beta$ LG/LF coacervates were prepared under optimal coacervation conditions, i.e. at pH 5.5 and 0.01 mol/L ionic strength and separated from diluted phase. Dynamic apparent viscosity was determined by flow experiments under a wide shear rate range. The viscoelastic properties of the coacervated was proved using two techniques first the frequency sweep then the creep-recovery tests.

## 2. Materials and methods

### 2.1. Materials

LF with a purity of 90 g/100 g and iron saturation of 10–20 mol iron/mol protein according to technical specification was purchased from Fonterra Cooperative Group (Auckland, New Zealand). LF powder was used without further purification. Industrial bovine  $\beta$ LG containing both variants A and B was further purified before use. As  $\beta$ LG is prompt to self-aggregation during long storage, the non-native and aggregated species were regularly removed by acidic precipitation. The  $\beta$ LG powder was dispersed in ultrapure water (30 g/L), adjusted to pH 5.2 with 1 mol/L HCl and then kept at 30 °C for 10 min to precipitate aggregated and non-native forms. The dispersion was centrifuged at 36 000 g at 25 °C for 10 min (Avanti, J-26S XP BioSafe Three-Phase Non-IVD Centrifuge, Beckman Coulter, Villepinte, France). The supernatant containing native  $\beta$ -lactoglobulin (purity >95 g/100 g powder as assessed by HPLC) was adjusted to pH 7.0 with 1 mol/L NaOH, freeze-dried and stored at –20 °C until use. Whey protein isolate (WPI) was purchased from Lactalis Ingredients (Bourgbarré, France) and contained 84 g total proteins per 100 g of the powder. 2-(N-morpholino) ethane-sulfonic acid hydrate (MES) was purchased from Sigma-Aldrich (St. Louis, MO, USA) and all other chemicals were of analytical grade.

### 2.2. Preparation of heteroprotein coacervates

MES buffer 0.01 mol/L was prepared by solubilizing MES powder in ultra-pure water and adjusted to pH 5.5 by 1 mol/L NaOH solution. Protein powders were solubilized in 0.01 mol/L MES buffer adjusted at pH 5.5 using 1 mol/L HCl solution. This pH value was found to be

optimal for complex coacervation between the two whey proteins at chosen stoichiometry and total protein concentration (Chapeau et al., 2016). The protein concentrations were determined in these two stock solutions by absorbance at 280 nm (SAFAS UV MC2, Safas, Monaco) using 0.96 L/g.cm and 1.47 L/g.cm as extinction coefficients for  $\beta$ LG and LF, respectively.

In order to prepare the coacervates, The optimised protocol published previously was applied (Chapeau et al., 2017). Briefly, an equivalent volume of the two protein solutions were mixed at room temperature to reach a final concentration of 0.5 mmol/L and 0.05 mmol/L for  $\beta$ LG and LF, respectively, which means a  $\beta$ LG/LF molar ratio of 10:1. Mechanical stirring was performed by stirring the solution in a vessel containing a propeller pale of 2.5 cm diameter, with three blades. The propeller was set in rotational motion by the mean of an electric motor set at 360 rpm. The spontaneous formation of coacervates as spherical droplets was monitored by turbidity measurements at 600 nm (SAFAS UV MC2, Safas, Monaco) and microscopic observations on a phase contrast microscope (BX51TF, Olympus, Rungis, France). This mixture was stored for 12 h and then centrifuged at 37 000 g for 30 min at 20 °C in order to separate the two liquid phases and extract the coacervate phase. From an experiment to another, a coacervation yield of 55–65 g of proteins in the coacervates/100 g initial total proteins was recovered. For each experiment, a total volume of 100 mL was implemented to get about 0.7–0.9 g of the coacervates enough to perform 3 to 4 rheological measurements. After centrifugation, the protein content in the coacervates phase was quantified by HPLC as previously reported (Chapeau et al., 2017). About 25–30 g of proteins were quantified for 100 g of recovered hydrated coacervates.

### 2.3. Rheological measurements

Rheological measurements of the coacervates were carried out using a stress-controlled rheometer (DHR2, TA Instruments, Guyancourt, France) with a cone - plate geometry (angle of 2°, diameter = 20 mm, truncature = 51.5  $\mu$ m) and a parallel plate geometry (diameter = 20 mm) with gap values of 250  $\mu$ m and 500  $\mu$ m.

Whatever geometry is used, around 200 mg of coacervates samples were loaded on the Peltier plate at 20 °C and allowed to rest for 2 min before measurement.

All rheology measurements were performed at least twice and plotted as means and standard deviations and fitting of data was performed with python (version: 3.9.5) and excel software.

#### 2.3.1. Flow measurements

Flow measurements were performed in an upward shear rate sweep (0.01–300 s<sup>-1</sup>) followed by a downward one. Measurements were performed by averaging for 20 s after an equilibrium time of 100 s at low shear rates (0.01–0.1 s<sup>-1</sup>) and for 5 s after 10 s equilibrium at higher shear rates (0.1–300 s<sup>-1</sup>). All the flow measurements were performed using a cone - plate geometry and a parallel plate geometry.

#### 2.3.2. Flow measurement plus constant shear rate

Flow experiment was performed as above in a cone-plate geometry, but once a shear rate of 1 s<sup>-1</sup> was reached during the upward and downward sweep, this shear rate was maintained for 6 min and the viscosity was measured versus time.

#### 2.3.3. Frequency sweeps

Frequency sweeps were carried out from 100 to 0.1 Hz with an oscillatory strain amplitude of 0.001, which was in the linear viscoelastic regime, in a cone-plate geometry.

#### 2.3.4. Creep and recovery tests

Creep and recovery were conducted with a cone-plate geometry using stress values ( $\sigma$ ) of 0.5–5 Pa for 10 min each.

### 3. Results and discussion

Fig. 1 illustrates the steps of liquid-liquid phase separation that led to the formation of  $\beta$ LG/LF complex coacervates. The process starts with spontaneous increase of solution turbidity to reach  $2.8 \pm 0.15 \text{ cm}^{-1}$ , a characteristic value of complex coacervation between these two whey proteins in solution (Chapeau et al., 2016; Yan et al., 2013). The spontaneous formation of spherical droplets, with a mean diameter between 5 and 10  $\mu\text{m}$ , a signature of the complex coacervation process was attested by phase contrast microscopy (Fig. 1B). The spontaneous formation of these droplets corresponds to the microphase separation step of the complex coacervation process. The coalescence of the droplets leads to the macrophase separation at the end as indicated by the white arrow (Fig. 1A). The coacervation yield obtained at used total protein concentration of 13 g/L varied from 55 to 60 g of proteins in the coacervates/100 g initial total proteins, as already described in details (Chapeau et al., 2016).

#### 3.1. Flow

As a first experiment, the apparent viscosities at low shear rates were measured (Fig. 2). The plot showed a behaviour close to Newtonian fluids, with a slight decrease in viscosity at increasing rates, with increasing and decreasing steps almost superimposed. Consistency and behaviour indexes from the power law were  $K = 51.9 \pm 0.9 \text{ Pa}\cdot\text{s}^n$  and  $n = 0.94 \pm 0.03$ , respectively, confirming a behaviour index close to 1. Given that  $\beta$ LG is the main component of whey protein isolates (WPI) and also the major protein in the  $\beta$ LG/LF coacervates phase (Peixoto et al., 2016), The viscosity of coacervates was compared with that of a WPI solution at the same pH and total protein concentration of 250 g/L. At this concentration, WPI shows homogeneous solution with no phase separation nor coacervation. Using the same protocol, WPI solution exhibited a Newtonian behaviour with a viscosity value of  $23 \pm 0.5 \text{ mPa}\cdot\text{s}$  at  $10 \text{ s}^{-1}$  (data not shown), a value 2000–3000 times lower than the viscosity of  $\beta$ LG/LF coacervates at  $10 \text{ s}^{-1}$ . This high difference underlines that the internal organisation/interaction play a major role in the rheological properties of the coacervates network, which deserves to be studied in-depth.

The apparent viscosities of  $\beta$ LG/LF coacervates in a much wider shear rates range is shown in Fig. 3. For higher shear rates, the dynamic viscosity decreased sharply and it showed a high hysteresis between the upward and downward steps. Despite the dramatic decrease of the viscosity during the upward shear rate, the initial viscosity of the

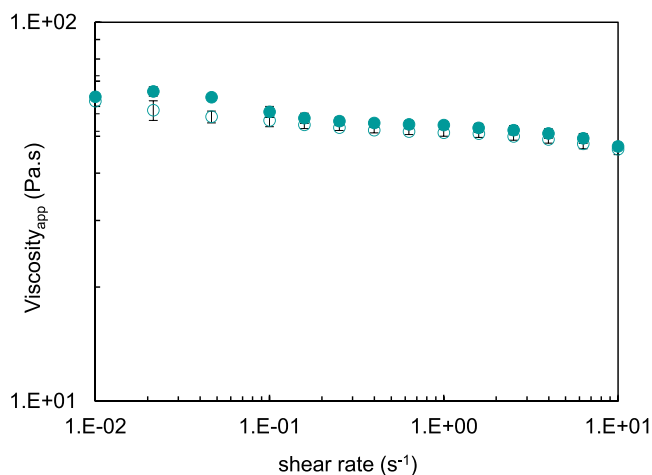


Fig. 2. Apparent viscosity of coacervates at strain rates from 0.01 to  $10 \text{ s}^{-1}$  as measured at  $20 \text{ }^\circ\text{C}$ . Values from three preparation of coacervates with cone-plate geometry. Close symbols: upward shear rate; open symbols: downward shear rate. Mean and standard deviations from three measurements are plotted.

coacervates was fully recovered by the end of the flow cycle. This behaviour was similar with the cone-plate and the plate-plate geometry, although the viscosity was slightly lower with the plate-plate than with the cone-plate geometry and the hysteresis loop was slightly larger with the cone than with the plate. Similar behaviour has been already reported for other coacervates systems: whey protein/gum Arabic coacervates at pH 4 above a critical shear rate of  $30 \text{ s}^{-1}$  (Weinbreck, Wientjes, Nieuwenhuijse, Robijn, & de Kruif, 2004), ovalbumin-gum Arabic coacervates at pH 2.7–3.7 above  $5 - 10 \text{ s}^{-1}$  (Niu et al., 2018) and polyelectrolyte/surfactant coacervates (Liberatore, Wyatt, Henry, Dubin, & Foun, 2009; Liu, Morishima, & Winnik, 2002).

To better understand what happened between 1 and  $300 \text{ s}^{-1}$ , an extra experiment was performed during the flow measurement. The experiment of Fig. 3 was duplicated but at  $1 \text{ s}^{-1}$  the viscosity was measured as a function of time during the upward and the downward flow. Fig. 4 shows the obtained results at constant shear rate experiment at  $1 \text{ s}^{-1}$ . During the upward flow curve, the viscosity remained constant, meaning that the coacervates was in an equilibrium state. However, in the downward flow curve, the viscosity increased over time. This

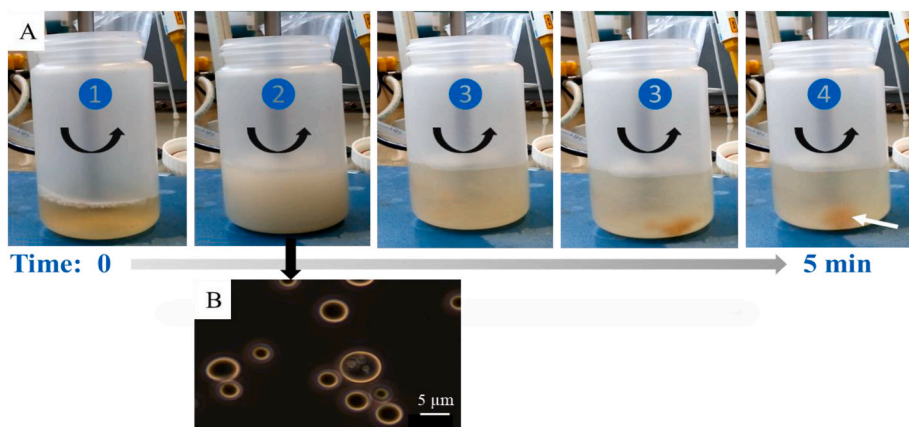
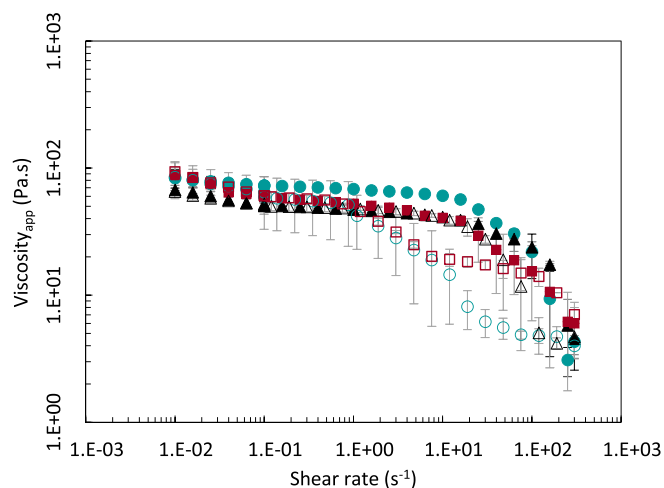
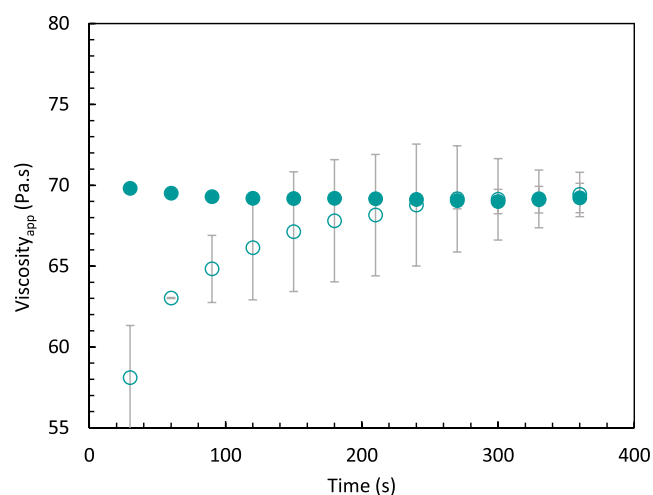


Fig. 1. A- Visual monitoring over time of the liquid-liquid phase separation i.e. complex coacervation between lactoferrin and  $\beta$ -lactoglobulin under continuous stirring in 0.01 mol/L MES buffer pH 5.5. Total batch mixing volume = 100 mL. ①: Solution of lactoferrin at 0.05 mmol/L; ② At  $t_0$ , addition of 0.5 mmol/L  $\beta$ -lactoglobulin solution with spontaneous appearance of turbidity. This step corresponds to the microphase separation of complex coacervation with the formation of micrometric droplets (B), characteristic of the coacervation process; ③: Initiation and progression of liquid-liquid phase separation; ④: Macrophase separation with the formation of coacervates indicated by the white arrow.



**Fig. 3.** Apparent viscosity of  $\beta$ LG/LF coacervates as a function of shear rate from  $0.01 \text{ s}^{-1}$  to  $300 \text{ s}^{-1}$  at  $20 \text{ }^\circ\text{C}$ . Cone-plate ( $\bullet$ ) (three measurements), plate-plate gap =  $250 \text{ }\mu\text{m}$  ( $\blacktriangle$ ) (two measurements), plate-plate gap =  $500 \text{ }\mu\text{m}$  ( $\blacksquare$ ) (two measurements). Close symbols: upward shear rate; open symbols: downward shear rate. Mean and standard deviations of all measurements are plotted.



**Fig. 4.** Apparent viscosity of  $\beta$ LG/LF coacervates as a function of time during a constant shear rate at  $1 \text{ s}^{-1}$ : upward flow curve (close circle) and downward flow curve (open circle). Mean and standard deviations from duplicate.

thixotropic behaviour was also observed in the case of coacervates made from protein/polysaccharide (Weinbreck et al., 2004; Niu et al., 2018) and from polyelectrolyte/surfactant (Liberatore et al., 2009; Liu et al., 2002). Weinbreck et al. explained the drop in viscosity above a critical shear rate as the one observed in Fig. 3 by a breakdown of the structure due to the breakup of physical bonds in the coacervates network at high shear. Once a critical shear rate is reached, the electrostatic interactions inside the protein network is weakened, which causes a change in the coacervates structure (Weinbreck et al., 2004). This behaviour was the same regardless of the selected geometry or the gap value in the plate-plate geometry. The breakdown of the structure at high shear rate was not due to an artefact from the geometry such as a non-laminar shear nor a wall slip of the sample but rather to the changes in the coacervates structure.

Hence, the disrupted coacervates was able to recover its initial structure during the downward flow in agreement with the hysteresis loop observed between increasing and decreasing flow rate (Fig. 3). The structural changes were fully reversible but needed time to reform and

restore similar original state of the network. This hypothesis is confirmed in Fig. 4 where the recovery of the coacervates structure brought about by the rearrangement of the physical bonds between  $\beta$ LG and LF was proved to be time dependent. These results were similar to those reported for the OVA-GA complex coacervates (Niu et al., 2018).

Alongside the hypothesis of a shear-induced breakdown of the coacervates structure, other assumptions could be invoked such as a microscale structural reorganization of the interspersed phases of the complex coacervates (Kaur, Weerasekare, & Stewart, 2011). This structural rearrangement is due to a temporary breaking up of the attractive interactions between two polymers aggregated in dense particles in the dispersion (Niu et al., 2018). Another assumption was giving by Liberatore et al. who explained the drop of the viscosity by a shear-induced phase separation; using a simultaneous characterisation by rheology and small angle light scattering they observed that, once the shear rate increases, a phase separation took place leading to a shear thinning behaviour of the coacervates (Liberatore et al., 2009). Another supposition could be related to the sample leaving the geometry gap under high shear rate that leads to a lower viscosity values. The possibility of shear banding at high shear rate should also be taken into account.

According to the latter authors, the Cross rheological model (Cross, 1965) described in equation (1) can fit the viscosity data:

$$\eta = \eta_{\infty} + \frac{\eta_0 - \eta_{\infty}}{1 + (\dot{\gamma}t)^m} \quad (1)$$

where  $\eta_0$  and  $\eta_{\infty}$  are the zero-shear and the high-shear viscosity, respectively,  $t$  is the relaxation time i.e. the inverse of the onset of shear thinning, the shear rate and  $m$  the shear thinning index, also known as the rate constant. A value of  $m$  equal to 0 means a Newtonian behaviour, whereas the higher the  $m$  value, the more intense the shear thinning behaviour. The fitting of the data gives a value of  $m$  equal to 0.53. According to Liberatore et al. (2009), a stress plateau is obtained at values of  $m$  equal to 1 or more. This plateau could be an indication of a possible shear banding in the geometry. Shear banding can originate from many behaviours, such as disentanglement of polymers, shear-induced phase separation due to spatial fluctuation of polymer concentrations, and particle scission and reformation dynamics. For the  $\beta$ LG/LF coacervates, a plateau of stress was hardly fitted with  $m$  adjusted to values around 0.5.

The aim of the flow experiments was to study the viscous properties of  $\beta$ LG/LF coacervates over a wide shear rate range.  $\beta$ LG/LF hetero-protein coacervates had two different behaviours depending on the shear rate applied; a Newtonian behaviour at low shear rates and a shear thinning behaviour above  $10 \text{ s}^{-1}$ . In addition to that, a hysteresis loop between the upward and downward flow was observed likely due to a slow and progressive recovery and reconstitution of electrostatic interactions inside the protein network. The weakness of electrostatic interactions could also lead to weak elasticity inside the coacervates structure therefore a study of the viscoelastic properties of the coacervates was carried out by frequency sweep measurements and creep-recovery tests.

### 3.2. Frequency sweeps

Fig. 5 shows the viscoelastic behaviour of  $\beta$ LG/LF coacervates at  $20 \text{ }^\circ\text{C}$ . Over the whole range of angular frequencies studied,  $G''$  dominated the behaviour, mostly at low frequencies where the value of  $G''$  was 10 times higher than  $G'$  which meant that the coacervates had a liquid-like behaviour. This behaviour is close to the one depicted on the coacervates between  $\beta$ LG and LF performed under other experimental conditions (Kizilay et al., 2014) as well as with others types of polyelectrolyte complexes (PECs) (Marciel, Srivastava, & Tirrell, 2018). Using a discrete fitting of relaxation times with the Maxwell model and plotting  $G'$  and  $G''$  for enlarged frequencies (TA Instruments utilities,

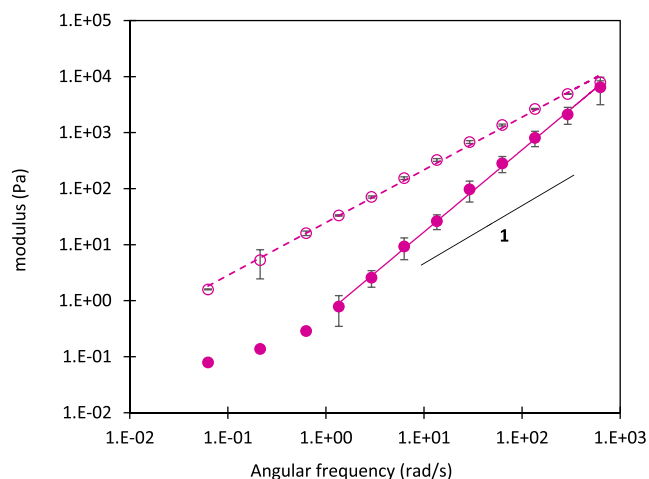


**Fig. 5.** Storage modulus (full symbols ■) and loss modulus (open symbols ●) of  $\beta$ LG/LF coacervates as function of angular frequency at 20 °C (two measurements). Solid line:  $G'$  frequency power law scaling above 1 rad/s. Dashed line:  $G''$  frequency power law scaling. Mean and standard deviations are plotted.

data not shown) allowed a raw estimation of the crossing frequency. The fitting generally required more than one single element, as usually for complex systems (Liu et al., 2002). Crossing frequencies were estimated at 760 rad/s. The interconnected structures responsible for the viscoelastic properties inside  $\beta$ LG/LF coacervates have a relaxation lifetimes around 8 ms. This value is of the same order of magnitude as determined for the same heteroprotein coacervates at pH 6 which was found to be 1 ms (Kizilay et al., 2014). A very low lifetime for interconnecting electrostatic interactions between polymers gives transient network properties, as it was shown, and a behaviour clearly dominated by viscous properties.

While  $G''$  was linearly dependent to the angular frequency during its whole range,  $G'$  trend toward a plateau and did not follow a linear fit in the low frequency regime. Both  $G'$  and  $G''$  thus followed a power law of frequency, for the  $G''$  with an exponent close to 1 ( $0.95 \pm 0.01$ ) and at frequencies larger than 1 rad/s for the  $G'$  with an exponent of  $1.47 \pm 0.01$ . Others have reported deviation from the typical Maxwellian behaviour of  $G'$  as a function of frequency. This deviation has been attributed either to a contribution of a distribution of relaxation times in the tested frequency domain, for instance between ion pairs considered as the sticky points of the transient network. (Ali & Prabhu, 2018; Bohidar, 2015) or to a limited sensibility of the rheometer at low frequencies (Boire et al., 2018; Marciel et al., 2018; Tang, Wang, & Olsen, 2015) or to the presence of a very weak elastic network (Bohidar, Dubin, Majhi, Tribet, & Jaeger, 2005; Dardelle & Erni, 2014). Sticky Rouse relaxation phenomenon has also been advanced to explain the behaviour in coacervates made from weak polyelectrolytes due in fact to the mobility of free non-interacting polyelectrolytes (Marciel et al., 2018; Tang et al., 2015). For a large number of coacervates involving oppositely charged molecules, low-salt environment results in stronger electrostatic interactions between ion pairs with higher solid-like properties, whereas high salt concentrations weakens ion-pair strength, leading to labile sticky connections and increased liquid-like properties (Bohidar, 2015; Chai, Lee, & Huang, 2014; Liu, Momani, Winter, & L.Perry, 2017; Liu, Winter, & Perry, 2017; Xiong et al., 2017). However an inverted effect of salt has also been reported (Priftis, Megley, Laugel, & Tirrell, 2013) and pH can also alter the viscoelastic behaviour of coacervates (Kizilay et al., 2014; Marciel et al., 2018; Raeli, Rafe, & Shahidi, 2018; Weinbreck et al., 2004). All these effects act by modulating the strength of electrostatic interactions between the two polymers in the coacervates phase. Peixoto et al. (2016) reported on the composition, dynamic and internal structure of  $\beta$ LG/LF coacervates

using solid-state NMR experiments combined with in silico docking. In particular, the co-existence of three types of molecular entities with specific dynamics and  $R_h$  properties has been shown in the current coacervates network. The smaller one is assigned to  $\beta$ LG2 and  $\beta$ LG monomers ( $R_h = 2$  nm), which is used in excess in the initial mixture. The other entities with  $R_h$  of 7 nm and  $\approx 30$ –60 nm are assigned to heterocomplexes involving LF and  $\beta$ LG2, the association of which built the overall “skeleton of the coacervates” (Peixoto et al., 2016). The high mobility of some of these species and the weak connectivity between them could explain the observed viscoelastic properties of the overall network of  $\beta$ LG/LF heteroprotein coacervates.

### 3.3. Creep-recovery tests

Fig. 6a reports the plot of strain versus time at various stress values. Once the stress was applied, the coacervates underwent deformation without an instantaneous elastic response. However, in the recovery test, two different behaviours were noticed: the coacervates had a slight recovery at 0.5 and 1 Pa, whereas the recovery was hardly detectable at higher applied stress. The coacervates thus showed a viscoelastic response at low stress values, but only a liquid-like behaviour under higher stress. This result agrees with a dominant liquid-like behaviour of the coacervates with the possible presence of a very weak elastic

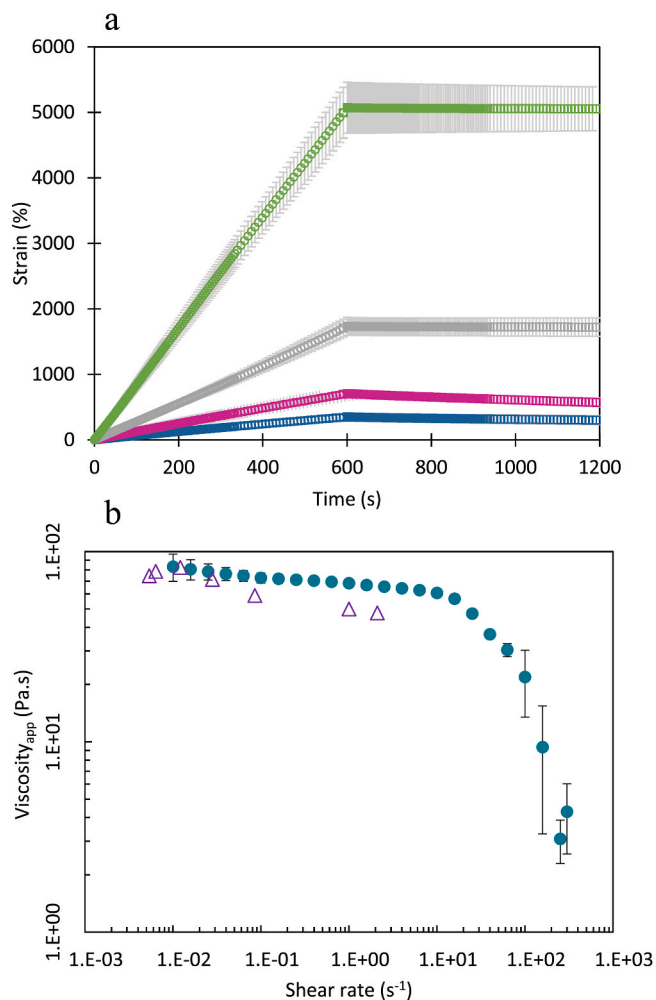


**Fig. 6.** a- Strain versus time in creep (0–600 s) and recovery test (600–1200 s) of  $\beta$ LG/LF coacervates at 20 °C. Applied stress: 0.5 Pa (■), 1 Pa (■), 2 Pa (■) and 5 Pa (■). b- Apparent viscosity of  $\beta$ LG/LF coacervates as function of shear rate in flow (●) and creep tests (△). Mean and standard deviations from four measurements.

network as previously hypothesis in other coacervated systems (Bohidar et al., 2005) with mechanical spectra showing a turn in  $G'$  at low frequency. The observed viscoelastic behaviour at low stress is consistent with the results reported for the gum Arabic/whey protein isolate coacervates and gum Arabic/chitosan coacervates (Tavares & Noreña, 2019; 2020) for applied stress  $<1$  Pa and for fish gelatine and sodium alginate complexes (Derkach, Kolotova, Voron'ko, Obluchinskaya, & Malkin, 2021).

Applying high stress values for 10 min might cause a breakdown in the protein network, which caused a reorganization in the coacervates structure and therefore a loss of the weak elasticity.

$J(t)$  defines the creep compliance  $J(t) = \frac{\sigma}{\varepsilon(t)}$ . The coacervates had a liquid-like dominant behavior, which meant that the creep compliance would be a linear function of time ( $t$ ) as mentioned in equation (2):

$$J(t) = a.t \quad (2)$$

The creep compliance versus time plots were linear (not shown) and their slopes allowed the evaluation of the dynamic viscosity at their respective strain rates. Fig. 6b shows the comparison of the viscosity of the coacervates measured in the flow and creep tests. Viscosity results are in reasonably good agreement and confirmed the liquid-like dominant behaviour of the current coacervates. The behaviour under creep-recovery tests of coacervates made from oppositely charged proteins is clearly elucidated here for the first time.

#### 4. Conclusion

The aforementioned results clearly demonstrated the exceptional rheological properties of complex coacervates made from two oppositely charged proteins  $\beta$ LG and LF. A dominant liquid-like behavior is demonstrated, together with the presence of a weak elastic network probably due to electrostatic interactions between  $\beta$ LG and LF, and responsible for shear thinning and thixotropy in the flow behavior and to non-Maxwellian and non-zero recovery behavior in oscillation and creep-recovery tests. The formed coacervates, composed of 250 g of proteins/kg, constitute a hydrated network with exceptional viscosity close to 60 Pa.s, while the viscosity of individual proteins at equivalent concentration is of the order of a few mPa.s. The observed rheological properties are the result of weak and reversible interactions. Hence, the combination of the rheological methods used here allowed for the understanding the behavior of heteroprotein coacervates and to the best of our knowledge, this is the first time that such in-depth characterization is reported. Information on the composition and the physical properties of heteroprotein coacervates is very useful for identifying and exploring their potentials for specific applications including encapsulation and protection of bioactive molecules but also in controlling the texture of protein enriched food formulations. Studies on how the rheological properties of heteroprotein coacervates can be tuned by changes in ionic strength and temperature are in progress.

#### CRedit authorship contribution statement

**Rima Soussi Hachfi:** Execution of experiments, Investigation, Methodology, Formal analysis, Writing. **Marie-Hélène Famelart:** Supervision, Proposition of experiments, Validation, Formal analysis, writing-Review. **Florence Rousseau:** Execution of experiments, Methodology, Formal analysis. **Pascaline Hamon:** Execution of experiments, Methodology, Investigation. **Saïd Bouhallab:** Conceptualization, Supervision, Project supervision, Writing – review & editing.

#### Declaration of competing interest

The authors declare no conflicts of interest.

#### Acknowledgements

We gratefully acknowledge the financial support provided by the Regional council of Brittany and INRAE.

#### References

- Abraham, J., Sharika, T., Mishra, R. K., & Thomas, S. (2017). Rheological characteristics of nanomaterials and nanocomposites. In *Micro and nano fibrillar composites (MFCs and NFCs) from polymer blends* (pp. 327–350). Elsevier. <https://doi.org/10.1016/B978-0-08-101991-7.00014-5>.
- Ali, S., & Prabhu, V. (2018). Relaxation behavior by time-salt and time-temperature superpositions of polyelectrolyte complexes from coacervate to precipitate. *Gels*, 4(1), 11–23.
- Anema, S. G., & de Kruijff, C. G. (2014). Complex coacervates of lactotransferrin and  $\beta$ -lactoglobulin. *Journal of Colloid and Interface Science*, 430, 214–220.
- Blocher, W. C., & Perry, S. L. (2017). Complex coacervate-based materials for biomedicine. *WIREs Nanomedicine and Nanobiotechnology*, 9, e1442.
- Bohidar, H. B. (2015). *Fundamentals of polymer physics and molecular biophysics*. Cambridge UK: Cambridge University Press.
- Bohidar, H., Dubin, P. L., Majhi, P. R., Tribet, C., & Jaeger, W. (2005). Effects of Protein–Polyelectrolyte affinity and polyelectrolyte molecular weight on dynamic properties of bovine serum Albumin–Poly(diallyldimethylammonium chloride) coacervates. *Biomacromolecules*, 6(3), 1573–1585.
- Boire, A., Bouchoux, A., Bouhallab, S., Chapeau, A.-L., Croguennec, T., Ferraro, V., et al. (2018). Proteins for the future: A soft matter approach to link basic knowledge and innovative applications. *Innovative Food Science & Emerging Technologies*, 46, 18–28.
- Bungenberg De Jong, H. G., & Kruyt, H. R. (1929). Coacervation (partial miscibility in colloid systems). *Proceedings of the Royal Academy of Science at Amsterdam*, 32, 849–856.
- Chai, C., Lee, J., & Huang, Q. (2014). The effect of ionic strength on the rheology of pH-induced bovine serum albumin/k-carrageenan coacervates. *Lebensmittel-Wissenschaft und -Technologie- Food Science and Technology*, 59(1), 356–360.
- Chapeau, A.-L., Hamon, P., Rousseau, F., Croguennec, T., Poncelet, D., & Bouhallab, S. (2017). Scale-up production of vitamin loaded heteroprotein coacervates and their protective property. *Journal of Food Engineering*, 206, 67–76.
- Chapeau, A.-L., Tavares, G. M., Hamon, P., Croguennec, T., Poncelet, D., & Bouhallab, S. (2016). Spontaneous co-assembly of lactoferrin and  $\beta$ -lactoglobulin as a promising biocarrier for vitamin B9. *Food Hydrocolloids*, 57, 280–290.
- Croguennec, T., Tavares, G. M., & Bouhallab, S. (2017). Heteroprotein complex coacervation: A generic process. *Advances in Colloid and Interface Science*, 239, 115–126.
- Cross, M. M. (1965). Rheology of non-Newtonian fluids: A new flow equation for pseudoplastic systems. *Journal of Colloid Science*, 20, 417–437.
- Dardelle, G., & Ermi, P. (2014). Three-phase interactions and interfacial transport phenomena in coacervate/oil/water systems. *Advances in Colloid and Interface Science*, 206, 79–91.
- Derkach, S. R., Kolotova, D. S., Voron'ko, N. G., Obluchinskaya, E. D., & Malkin, A. Y. (2021). Rheological properties of fish gelatin modified with sodium alginate. *Polymers*, 13(5), 743–760.
- Jho, Y., Yoo, H. Y., Lin, Y., Han, S., & Hwang, D. S. (2017). Molecular and structural basis of low interfacial energy of complex coacervates in water. *Advances in Colloid and Interface Science*, 239, 61–73.
- Kapelner, R. A., Yeong, V., & Obermeyer, A. C. (2021). Molecular determinants of protein-based coacervates. *Current Opinion in Colloid & Interface Science*, 52, Article 101407.
- Kaur, S., Weerasekare, G. M., & Stewart, R. J. (2011). Multiphase Adhesive coacervates inspired by the sandcastle worm. *ACS Applied Materials & Interfaces*, 3(4), 941–944.
- Kizilay, E., Kayitmazer, A. B., & Dubin, P. L. (2011). Complexation and quaternization of polyelectrolytes with oppositely charged colloids. *Advances in Colloid and Interface Science*, 167(1–2), 24–37.
- Kizilay, E., Seeman, D., Yan, Y., Du, X., Dubin, P. L., Donato-Capel, L., et al. (2014). Structure of bovine  $\beta$ -lactoglobulin-lactoferrin coacervates. *Soft Matter*, 10(37), 7262–7268.
- Liberatore, M. W., Wyatt, N. B., Henry, M., Dubin, P. L., & Foun, E. (2009). Shear-induced phase separation in polyelectrolyte/mixed micelle coacervates. *Langmuir*, 25(23), 13376–13383.
- Liu, Y., Momani, B., Winter, H. H., & Perry, S. L. (2017). Rheological characterization of liquid-to-solid transitions in bulk polyelectrolyte complexes. *Soft Matter*, 13(40), 7332–7340.
- Liu, R. C. W., Morishima, Y., & Winnik, F. M. (2002). Rheological properties of mixtures of oppositely charged polyelectrolytes. A study of the interactions between a cationic cellulose ether and a hydrophobically modified poly[sodium 2-(acrylamido)-2-methylpropanesulfonate]. *Polymer Journal*, 34(5), 340–346.
- Liu, Y., Winter, H. H., & Perry, S. L. (2017). Linear viscoelasticity of complex coacervates. *Advances in Colloid and Interface Science*, 239, 46–60.
- Marciel, A. B., Srivastava, S., & Tirrell, M. V. (2018). Structure and rheology of polyelectrolyte complex coacervates. *Soft Matter*, 14, 2454–2464.
- Niu, F., Kou, M., Fan, J., Pan, W., Feng, Z.-J., Su, Y., et al. (2018). Structural characteristics and rheological properties of ovalbumin-gum Arabic complex coacervates. *Food Chemistry*, 260, 1–6.
- Peixoto, P. D. S., Tavares, G. M., Croguennec, T., Nicolas, A., Hamon, P., Roiland, C., et al. (2016). Structure and dynamics of heteroprotein coacervates. *Langmuir*, 32(31), 7821–7828.

- Priftis, D., Megley, K., Laugel, N., & Tirrell, M. (2013). Complex coacervation of poly (ethylene-imine)/polypeptide aqueous solutions: Thermodynamic and rheological characterization. *Journal of Colloid and Interface Science*, 398, 39–50.
- Raei, M., Rafe, A., & Shahidi, F. (2018). Rheological and structural characteristics of whey protein-pectin complex coacervates. *Journal of Food Engineering*, 228, 25–31.
- Tang, S., Wang, M., & Olsen, B. D. (2015). Anomalous self-diffusion and sticky rouse dynamics in associative protein hydrogels. *Journal of the American Chemical Society*, 137(11), 3946–3957.
- Tavares, G. M., Croguennec, T., Hamon, P., Carvalho, A. F., & Bouhallab, S. (2015). Selective coacervation between lactoferrin and the two isoforms of  $\beta$ -lactoglobulin. *Food Hydrocolloids*, 48, 238–247.
- Tavares, L., & Noreña, C. P. Z. (2019). Encapsulation of garlic extract using complex coacervation with whey protein isolate and chitosan as wall materials followed by spray drying. *Food Hydrocolloids*, 89, 360–369.
- Tavares, L., & Noreña, C. P. Z. (2020). Encapsulation of ginger essential oil using complex coacervation method: Coacervate formation, rheological property, and physicochemical characterization. *Food and Bioprocess Technology*, 13(8), 1405–1420.
- Wang, X., Zhang, P., & Tian, L. (2021). Spatiotemporal organization of coacervate microdroplets. *Current Opinion in Colloid & Interface Science*, 52, Article 101420.
- Weinbreck, F., Wientjes, R. H. W., Nieuwenhuijse, H., Robijn, G. W., & de Kruif, C. G. (2004). Rheological properties of whey protein/gum Arabic coacervates. *Journal of Rheology*, 48(6), 1215–1228.
- Xiong, W., Ren, C., Tian, M., Yang, X., Li, J., & Li, B. (2017). Complex coacervation of ovalbumin-carboxymethylcellulose assessed by isothermal titration calorimeter and rheology: Effect of ionic strength and charge density of polysaccharide. *Food Hydrocolloids*, 73, 41–50.
- Yan, Y., Kizilay, E., Seeman, D., Flanagan, S., Dubin, P. L., Bovetto, L., et al. (2013). Heteroprotein complex coacervation: Bovine  $\beta$ -lactoglobulin and lactoferrin. *Langmuir*, 29(50), 15614–15623.
- Yewdall, N. A., André, A. A. M., Lu, T., & Spruijt, E. (2021). Coacervates as models of membraneless organelles. *Current Opinion in Colloid & Interface Science*, 52, Article 101416.
- Zheng, J., Tang, C., & Sun, W. (2020). Heteroprotein complex coacervation: Focus on experimental strategies to investigate structure formation as a function of intrinsic and external physicochemical parameters for food applications. *Advances in Colloid and Interface Science*, 284, Article 102268.